

N O T I C E

THIS DOCUMENT HAS BEEN REPRODUCED FROM
MICROFICHE. ALTHOUGH IT IS RECOGNIZED THAT
CERTAIN PORTIONS ARE ILLEGIBLE, IT IS BEING RELEASED
IN THE INTEREST OF MAKING AVAILABLE AS MUCH
INFORMATION AS POSSIBLE

UF
NASA Technical Memorandum 81563

(NASA-TM-81563) EFFECT OF LOAD, AREA OF
CONTACT, AND CONTACT STRESS ON THE WEAR
MECHANISMS OF A BONDED SOLID LUBRICANT FILM
(NASA) 22 p HC A02/MF A01 CSCL 11H

N81-12226

Unclass

G3/27 29320

EFFECT OF LOAD, AREA OF CONTACT, AND CONTACT STRESS ON THE WEAR MECHANISMS OF A BONDED SOLID LUBRICANT FILM

Robert L. Fusaro
Lewis Research Center
Cleveland, Ohio

Prepared for the
Third International Conference on Wear of Materials
sponsored by the American Society of Mechanical Engineers
San Francisco, California, March 30 - April 1, 1981

NASA



ABSTRACT

A pin-on-disk type of friction and wear apparatus was used to study the effect of load, contact stress and rider area of contact on the friction and wear properties of polyimide-bonded graphite fluoride films. Different rider area contacts were obtained by initially generating flats (with areas of 0.0035, 0.0071, 0.0145, and 0.0240 cm²) on 0.476-cm radius hemispherically-tipped riders. Different projected contact stresses were obtained by applying loads of 2.5- to 58.8-N to the flats. Two film wear mechanisms were observed. The first was found to be a linear function of contact stress and was independent of rider area of contact. The second was found to increase exponentially as the stress increased. The second also appeared to be a function of rider contact area. Wear equations for each mechanism were empirically derived from the experimental data. In general, friction coefficients increased with increasing rider contact area and with sliding duration. This was related to the build-up of thick rider transfer films.

INTRODUCTION

It has been shown in previous studies (1,2) that polyimide and polyimide bonded graphite fluoride films have potential for solid lubrication applications (such as foil bearings (3-7)) where long thermal soaks are encountered. Low weight loss rates, good adhesion, and good friction and wear properties were obtained for films thermally exposed at temperatures to 315° C.

In order to obtain a better understanding of the lubrication and wear mechanisms of polyimide-bonded graphite fluoride films, a hemispherically tipped rider (8) and a rider with a 0.95-mm-diameter flat on it (9) were slid against the film. In general, two stages (or regimes) of lubrication were identified. In the first stage, the film supported the load and the lubricating mechanism appeared to be shear (plastic flow) in a thin layer of the film between the bulk of the film and the metallic rider. In the second stage (which occurred after the original film had worn through to the metallic substrate), the lubricating mechanism appeared to be the shear of very thin solid lubricant films between the flat area on the rider and flat plateaus generated on the metallic asperities in the film wear track.

For the hemispherically tipped rider, the first stage of lubrication lasted only a very short time (<15 kc of sliding). However, for the 0.95-mm-diameter flat sliding on the film, the first stage lasted about 3500 kc. The reason for this vast difference was believed to be caused by the very high projected contact stresses imparted by the hemisphere. Under light stresses the wear process consisted mainly of the spalling of thin layers of the film (>2 μm); however, under the higher stresses created by the hemisphere, cracks were generated which propagated through the bulk film and led to the crumbling and complete break-up of the film on the wear track.

This study was conducted to investigate the effect of projected contact stress in more detail, and to determine if rider area of contact affected the wear rate. To do this, a pin-on-disk apparatus was used with hemispherically tipped pins which had 0.67, 0.95, 1.36, and 1.75-mm diameter flats on them. Loads of 2.5, 4.9, 9.8, 14.7, 19.6, 29.4, 34.3, 39.2, and 58.8 N were applied to the flats which slid against the films at 1000 rpm in a 50% R.H. air atmosphere.

MATERIALS

Pyralin polyimide (PI-4701) was used in this study. The polyimide was obtained as a thick precursor solution containing 43 percent solids. For a sprayable mixture, a thinner consisting of N-methylpyrrolidone and xylene was added. The polyimide-bonded graphite fluoride films were prepared by mixing equal parts by weight of polyimide solids with graphite fluoride powder. The graphite fluoride used had a fluorine-to-carbon ratio of 1.1. The films were applied to AISI 440C HT steel disks (1.2 cm thick by 6.3 cm in diam) that had a hardness of Rockwell C-58. The riders used in the friction and wear tests were also made from the AISI 440C HT steel with a hardness of Rockwell C-58.

FRICTION APPARATUS

A conventional type of pin-on-disk friction and wear apparatus was used in this study (Fig. 1); but the riders were 0.476 cm-radius hemispherically tipped pins with 0.67, 0.95, 1.36 or 1.75 mm-diameter flats worn on them (see insert Fig. 1). The flats gave projected contact areas of 0.0035, 0.0071, 0.0145 and 0.0240 cm², respectively.

The flat areas were loaded against the films (which were applied to a flat, 6.3-cm-diam disk) with dead weights of 2.5 to 58.8 N. The disks were rotated at 1000 rpm, and the rider slid on the disk at a radius of 2.5 cm which gave it a linear sliding speed of 2.6 m/sec. The friction specimens were enclosed in a chamber so that atmosphere could be controlled. To obtain a controlled air atmosphere of 10,000 ppm H₂O (~50% relative humidity), dry air and dry air bubbled through water were mixed. The humidity was monitored continuously. The rise in temperature on the film wear track due to frictional heating was monitored continuously by an infrared pyrometer.

PROCEDURE

Generation of Rider Flats

The flats on the 0.476 cm-radius hemispherically tipped riders (pins) were generated prior to conducting the friction and wear experiments by sliding them against a rubbed graphite fluoride film (which was applied to a sandblasted AISI 440C HT stainless steel disk). The rider was not removed from the holder after the flat was generated or while it was cleaned; and it and the disk (with applied polyimide-bonded

graphite fluoride film) were positioned and indexed in the apparatus by using a linear variable differential transformer (LVDT) so that a flat-on-flat configuration occurred with minimal misalignment being introduced (Fig. 1).

Surface Preparation and Cleaning

The disk surfaces were roughened by sandblasting to a centerline average (cla) roughness of 0.9 to 1.2 micrometers. After surface roughening, the disks were scrubbed with a brush under running tap water. The disks were rinsed in distilled water and then clean, dry compressed air was used to quickly dry the surfaces. The disks were stored in a dessicator until they were ready for coating with the solid lubricant.

The rider was lightly scrubbed with ethyl alcohol and with levigated alumina to remove the graphite fluoride transfer film that originated during the generation of the flat wear area. It was next rinsed in distilled water and dried with compressed air. Lubricant was not applied to the riders.

Film Application

An artist's arbrush was used to apply the polyimide-bonded graphite fluoride films to the disks. Because the film did not dry rapidly, only a thin layer was applied at one time in order to prevent "running". Each thin layer was cured completely before the next layer was applied. The cure consisted of heating the films at 100° C for 1 hour followed by 300° C for 2 hours.

The film thicknesses evaluated in this study were up to 39 micrometers (0.0015 in.). Since each layer applied was from 7 to 13 micrometers thick, up to five applications were needed to achieve the desired thicknesses.

Friction and Wear Tests

The procedure for conducting the friction and wear tests was as follows: The test specimens were inserted into the friction apparatus and the test chamber sealed. A controlled moist air test atmosphere (10,000 ppm H₂O) was purged through the chamber for 15 minutes before each test and continuously throughout the test. After purging, the disk was rotated at 1000 rpm and a the load gradually applied. The test temperature was 25° C.

Each test was stopped after 1/4 kilocycle (1/4 min) of sliding, and the rider and disk were removed from the friction apparatus the contact areas were examined by optical microscopy and photographed. Surface profiles of the disk wear tracks were also taken. The rider and disk were then placed back into the apparatus, and the test procedure was repeated. The rider was not removed from the holder, and locating pins in the apparatus insured that it was returned to its original position. The same was true for the disk.

Each test was stopped and the previous test procedure was repeated after selected sliding durations. Film wear was calculated by measuring the cross-sectional area of the polyimide bonded graphite fluoride film wear track (from the surface profiles) after each sliding interval. Rider wear was determined by measuring the change in the diameter of the wear scar on the hemispherically tipped rider and then calculating the volume of material worn away.

Analysis of Sliding Surfaces

Optical microscopy techniques were used to study the lubricating films, the transfer films, and the wear particles in this investigation. The surfaces were viewed at magnifications to 2000X. At these high magnifications, the depth of field was very small (ap-

prox. 1 μm); thus the focusing distance was used in measuring various features on the sliding surfaces such as film thickness, and wear track depth.

Polyimide-bonded graphite fluoride films were transparent when worn to a thickness of 1 μm or less. Since illumination and observation of the surfaces were normal to the surfaces, interference fringes could be seen in the films both on the disk wear track and on the rider. Inteferece fringes indicated when very thin solid lubricant films were present and gave an indication of their smoothness and continuity.

RESULTS AND DISCUSSION

Coefficient of Friction

The coefficient of friction for AISI 440C HT stainless steel riders sliding against polyimide (PI) - bonded graphite fluoride (CF_x)_n films is plotted as a function of sliding duration in Fig. 2. Since the riders had flat areas on them, different loads applied to the same flat area gave different values of contact stress, or the same load applied to different areas gave different values of stress. Figure 2 shows the effect of contact stress (pressure) on the friction coefficient for constant loads of 4.9 N (Fig. 2(a)), 9.8 N (Fig. 2(b)), 19.6 N (Fig. 2(c)), and 29.4 N (Fig. 2(d)). The contact stresses involved ranged from 2 MPa (300 psi) for the 4.9 N load applied to the 0.024 cm²-area flat to 56 MPa (8000 psi) for the 19.6 N load applied to the 0.0035 cm²-area flat.

Regardless of stress, load, or area of contact, the friction coefficient generally increased with increasing sliding duration. Also, it is seen that in general for constant load, the friction coefficient tended to increase as rider contact area increased or the rider contact stress decreased. To determine the effect or rider contact area and rider contact stress on the friction coefficient, friction coefficient values (from all tests) obtained after 60 and 500 kc of sliding are plotted in Fig. 3 as a function of rider area of contact and in Fig. 4 as a function of contact stress. The curves shown in Figs. 3 and 4 represent a linear regression fit (least squares) of the data. The curves indicate that the coefficient of friction tends to increase with increasing area of contact and to decrease with increasing rider contact stress.

The effect of temperature rise (due to frictional heating) on the friction coefficient was also investigated. Table I gives friction coefficient values and Table II gives the temperature rise on the film wear track due to frictional heating after various sliding intervals for all experimental conditions. Figure 5 shows plots of these data (friction coefficient versus film wear track temperature) for (a) 60 kc of sliding and (b) at the end of the experiments. The curves shown in the figure are linear regression fits to the data. The linear regression curves indicate that there is a very slight increase in friction coefficient due to frictional heating; however, the data scatter is so great that it is impossible to deduce that this is a real effect, especially for the data obtained at the end of the experiments (Fig. 5(b)).

Film Wear

Film wear was determined by taking surface profiles of the film wear track after various sliding intervals and measuring the cross-sectional area of material removed. Figure 6 compares surface profiles of the film wear tracks for four different rider contact areas after various sliding durations under a 9.8-N load. Because the vertical magnification of the profiles is about 50 times the horizontal magnification, the profiles are distorted by an exaggerated track depth.

At least 4 profiles at various points around the wear track were taken after various sliding durations and the wear areas averaged. For example, Fig. 7 plots the average cross-sectional area as a function of sliding duration for a 9.8-N load applied to the four different projected rider areas. The general trend for each test was for the film wear to increase in a linear manner as a function of sliding distance. For each individual test, wear (W) was found to be directly proportional to sliding distance (s), thus a wear equation of the form: $W = Rs$ could be assumed (12), where R is the wear rate. However, wear rate as seen in Fig. 7 was not solely dependent on load. Rider area of contact also influenced the film wear rate.

Figure 8 plots film wear as a function of sliding duration for a constant contact stress of 7 MPa (1000 psi) which was obtained by applying three different loads to three different rider contact areas. Comparing Fig. 8 to Fig. 7 indicates that the wear rate of the films is more dependent on contact stress than it is on total load.

Wear rate data for all experimental parameters used in this investigation are summarized in Tables III and IV. Table III gives a matrix comparison of the film wear rates as a function of load and rider contact area, and Table IV gives a comparison of the film wear rates as a function of contact stress and rider area of contact. The wear rates are expressed in terms of wear volume of material worn away per unit distance of sliding (m^3/m).

Table III shows that for a constant rider contact area, the film wear rate increased as load increased. The Table also shows that for constant load, the film wear rate decreased as the area of contact increased; indicating a contact stress (pressure) effect. Table IV shows for constant contact stress, the wear rate was either relatively constant or it increased with rider contact area; indicating a possible rider area of contact effect.

Figure 9 shows plots of average film wear rates as a function of contact stress. In Refs. 8 and 9, it was deduced that two different wear mechanisms could occur for PI-bonded (CF_x)_n films. The data of Fig. 9 tends to confirm that analysis, where a linear curve is seen and four other curves are seen departing from that curve at various values of contact stress.

It is believed the linear curve was caused by the first wear mechanism and the other curves were due to the second. The first wear mechanism was postulated to be due to the spalling of a very thin textured layer (<1 μm) at the surface of the film. The textured layer resulted from the polyimide and graphite fluoride plastically flowing and coalescing on the wear track of the film. Repeated passes over this layer caused it to blister and spall. As Fig. 9 illustrates, this wear mechanism seemed to be directly related to contact stress and not dependent on area of rider contact. The wear rate for the 1st wear mechanism (R_1) increased as contact stress (pressure) increased according to the relationship $R_1 = C_1P$, where C_1 is a constant and P is the contact stress in MPa. A linear regression fit of the data in Fig. 9 produced a wear equation for the 1st wear mechanism of

$$W_1 = R_1s = 1.2 \times 10^{-15} P s$$

where W_1 is expressed in m^3 and s in m.

The 2nd wear mechanism was postulated in Refs. 8 and 9 to be caused by defects in the bulk or by defects at the surface propagating into the bulk and causing rather large wear particles to be produced (up to 6 μm thick). The data of Fig. 9 indicate that both

contact stress and area of rider contact influenced the film wear rate of this mechanism.

To determine an equation for the wear rate for the 2nd wear mechanism, the wear rate values attributed to the first wear mechanism were subtracted from the total wear rate values given in Table IV. These values are plotted on semilog paper in Fig. 10 as a function of contact stress. A least squares exponential fit of the data produced a series of parallel exponential curves of the form $R_2 = C_A(1.3)^P$, where C_A is a constant that appeared to depend on the rider contact area (A). A least squares power fit of the four values of C_A as a function of rider contact area was made and $C_A = 3.1 \times 10^{-7} A^{0.2}$ where A is expressed in cm^2 . Thus, the wear equation for the second wear mechanism becomes:

$$W_2 = R_2s = 3.1 \times 10^{-7} A^{0.2} (1.3)^P s$$

The wear rate (R) for the values of contact stress (P) and rider contact area (A) used in this investigation thus becomes:

$$R = R_1 + R_2 = 1.2 \times 10^{-15} P + 3.1 \times 10^{-7} A^{0.2} (1.3)^P \text{ m}^3/\text{m}$$

The curves of Fig. 9 were plotted from this equation and show very good correlation with the experimental data.

The above equations were derived without considering any effect of frictional heating. Figure 11 plots film wear rate as a function maximum film wear track temperature. The figure tends to imply that the film wear rate increased as a function of increasing film wear track temperature. The figure may be misleading, however, since both the film wear rate and the film wear track temperature were dependent on load and contact area. If the Table I is compared to Table II, it is seen that for any particular constant load, a wide range of wear rates were obtained with no positive degree of correlation with the film wear track temperature. Thus, if a true effect of frictional heating does occur, it is clouded by the load and contact area effects.

Area of Contact Error Analysis

One problem in determining wear rates as a function of contact stress was determining the rider area of contact. When determining contact stress, constant area of rider contact was assumed; but the surface profiles of Fig. 6 indicate that as film wear occurred, the sides of the wear track also helped support the loads. In addition, the data of Ref. 9 showed that on initial contact, the rider flat only made contact with the tips of the film asperities, and that the area of contact of the rider with the film was about one fifth of the projected area of contact.

The effect that the wear track sides had on the true area measurements was not nearly as great as those caused by the film asperity interactions; and as the diameter of the flat area increased, the effect of the side support decreased. Figure 12 gives photomicrographs of three rider contact areas after various sliding intervals under a 9.8-N load, showing the contact areas made by the sides of the wear track.

The 0.0035 cm^2 -area flat is shown after 760 kc of sliding (Fig. 12(a)). The projected area of contact, due to the side support of the wear track, was found to be 0.0028 cm^2 , a 77% increase in contact area. The 0.0071 cm^2 -area flat is shown after 3500 kc of sliding (Fig. 12(b)). The side support area was 0.0032 cm^2 , a 46% increase in contact area. The 0.0145 cm^2 -area flat is shown after 4100 kc of sliding (Fig. 12(c)). The side support area was 0.0019 cm^2 , a 13% increase in area.

Undoubtedly, the contact at the sides of the wear track affected the film wear rate in some manner. However, the results indicate the effect was minimal since film wear increased at a relatively constant rate (Fig. 7).

What seemed to be most important were the initial conditions of load, contact stress and area of rider contact. These parameters determined whether thin, lamellar wear particles or large brittle-fracture wear particles were produced.

Rider Transfer and Wear

No measurable wear of the metallic rider flats occurred when sliding was completely on the PI-bonded $(CF_x)_n$ film. Only when the metallic substrate was reached, and the asperities of the substrate interacted with the rider was wear observed on the rider (9).

PI-bonded $(CF_x)_n$ transfer to the rider flat was found after all sliding intervals and under all sliding conditions. Initially (for all tests), transfer was very thin. Figure 13(a) shows a typical transfer film that occurred after 1 kc of sliding. This particular photograph is from the test which employed the 4.9-N load applied to the 0.0071 cm^2 -area flat. The transfer film was drawn in the direction of sliding and showed broad colorful interference bands where the transfer was thickest. The thickest transfer in this photograph was $0.8 \mu\text{m}$ (wavelength of red light).

As sliding duration progressed, the transfer to the rider flat tended to increase. In most cases, the transfer maintained its flowing nature and remained continuous and thin enough for interference bands to exit. Figure 13(b) shows transfer to the same rider flat after 6900 kc of sliding, indicating the change in transfer.

It was observed as the amount of transfer increased, so did the friction coefficient. For example, the friction coefficient for the test which employed the 4.9-N load sliding against the 0.0071 cm^2 -area flat after 1 kc of sliding was 0.12. As sliding continued and the transfer slowly built-up (Fig. 13), so did the friction coefficient (Fig. 2(a)); and after 6900 kc of sliding the friction coefficient was 0.20.

In a few instances, the friction coefficient went to values higher than 0.30. When this occurred, very heavy ridges of transfer were observed on the rider flat. An example of this is seen in Fig. 14, where a high magnification photomicrograph of the rider transfer which occurred to the 0.0145 cm^2 -area flat under a 4.9-N load after 7900 kc of sliding is seen. The transfer here is very thick (up to $9 \mu\text{m}$ thick) and does not show the colorful interference bands as were seen in the thinner transfer. The friction coefficient was 0.33. Even though friction seemed to increase with increasing transfer, no effect on wear was discernible. In general, however, thicker transfer films tended to occur on the larger area of contacts which indicates that the increase in film wear rate at lower stress levels for the larger diameter flats (Fig. 10) may be due to the heavier transfer.

CONCLUDING REMARKS

Very little information on the mechanisms of bonded-solid lubricant film lubrication, wear, and failure is available in the literature. In addition, most analytical expressions for the prediction of wear have been concerned with metallic surfaces or polymer solid bodies. Adhesive (10-12), abrasive (13-16), corrosive (17-18), fatigue (19-20), de-

lamination (21) and various other mechanisms of wear have been proposed (22), and analytical expressions formulated for each.

The results of this study and others conducted by the author (8,9,22,24) indicate that all these mechanisms can occur for the polyimide-bonded graphite fluoride films. Adhesion definitely takes place, this is evident from the thick transfer films observed. Abrasion often occurs, but this is usually due to a third body. A hard particle can embed itself into the film and abrade the metallic rider. The abraded rider can then abrade the film. Also sharp metallic substrate asperities can abrade the rider (after the film is worn through to the substrate). Results from Refs. 23 and 24 indicated the type of atmosphere in which the experiments were conducted markedly influenced the wear results, indicating a corrosive effect. This study shows that fatigue-like and delamination-like particles are produced in the first lubrication regime. Thus, the total wear picture is a complicated one.

Most of the wear theories stated above relate wear rate (wear volume per unit sliding distance) to the total load. Fatigue wear (19-20), however, is associated with contact stress (pressure). This study indicated the wear rate of PI-bonded $(CF_x)_n$ films was more dependent on contact stress than load; thus, it appears a fatigue type of wear process is the more prevalent type of wear taking place.

The analysis is complicated however, because two types of wear particles are produced, thin lamellar wear particles ($<1 \mu\text{m}$ thick) and brittle fracture type of wear particles ($>1 \mu\text{m}$ thick). The results of this paper indicated that the projected contact stress and the rider contact area determined the rate at which each type of particle was produced. For a constant rider area of contact, the transition from the first wear mechanism to the second wear mechanism seemed to be a gradual process (Fig. 9). Figure 15 shows high magnification photomicrographs of the film wear tracks after various sliding intervals for the 0.0071 cm^2 -area rider flat sliding on the film under loads of (a) 4.9-N, (b) 9.8-N, (c) 18.6-N, and (d) 29.4-N. The figure illustrates the effect of increasing contact stress on the film wear process. As the load or contact stress is increased, the wear track changed from a very smooth surface to one where large regions of cracking and spalling occurred.

SUMMARY OF RESULTS

Friction, wear, surface profilometry and optical microscopy studies of polyimide-bonded graphite fluoride films subjected to various load, various contact stresses, and various rider areas of contact indicate that:

1. At least two different wear mechanisms of the film occurred.

(a) The first was associated with the spalling of a thin textured layer at the surface of the film.

(b) The second was believed to be caused by defects in the bulk or at the surface propagating into the bulk and producing large wear particles.

2. Film wear for the first lubrication mechanism was found to be dependent on projected contact stress and independent of rider area of contact. A wear equation was derived from the experimental data and found to be $W_1 = 1.2 \times 10^{-15} P^3$, where W_1 is wear volume in m^3 , P is contact stress in MPa, and s is sliding distance in m.

3. Film wear for the second lubrication mechanism was found to be dependent on projected contact stress and rider area of contact. A wear equation derived from the experimental data was found to be

$W_2 = 3.1 \times 10^{-7} A^{0.2} (1.3)^{P_s}$, where W_2 is wear volume in m^3 for the second wear mechanism, and A is rider area of contact in cm^2 .

4. In general, the friction coefficient for each test increased with sliding duration; and the amount of transfer to the rider also increased with sliding duration. Thus, low friction coefficients were associated a thin layer-like type of transfer and high friction coefficients with a thick, heavy type of transfer:

5. No measurable wear occurred to the rider flats until the metallic substrate was contacted.

REFERENCES

1. Fusaro, R. L., "Effect of Thermal Exposure on Lubricating Properties of Polyimide Films and Polyimide-Bonded Graphite Fluoride Films," NASA TP-1125, 1978.
2. Fusaro, R. L., "Effect of Thermal Aging on the Tribological Properties of Polyimide Films and Polyimide Bonded Graphite Fluoride Films," Lubrication Engineering, Vol. 36, No. 3, Mar. 1980, pp. 143-153.
3. Bangs, S., "Foil Bearings Help Air Passengers Keep Their Cool," Power Transmission Design, Vol. 15, No. 2, Feb. 1973, pp. 27-31.
4. Blok, H., and Van Rossum, J. J., "The Foil Bearing - A New Departure in Hydrodynamic Lubrication," Lubrication Engineering, Vol. 9, No. 6, Dec. 1953, pp. 316-320.
5. Ma, J. T. S., "An Investigation of Self-Acting Foil Bearings," Journal of Basic Engineering, Vol. 87, No. 4, Dec. 1965, pp. 837-836.
6. Licht, L., "An Experimental Study of High-Speed Rotors Supported by Air-Lubricated Foil Bearings. Part I: Rotation in Pressurized and Self-Acting Foil Bearings," Journal of Lubrication Technology, Vol. 91, No. 3, July 1969, pp. 477-505.
7. Licht, L., and Branger, M., "Motion of a Small High-Speed Rotor in Three Types of Foil Bearings," Journal of Lubrication Technology, Vol. 97, No. 2, Apr. 1975, pp. 270-282.
8. Fusaro, R. L., "Lubricating and Wear Mechanisms for a Hemisphere Sliding on a Polyimide-Bonded Graphite Fluoride Film," NASA TP-1524, 1979.
9. Fusaro, R. L., "Lubrication and Wear Mechanisms of a Polyimide-Bonded Graphite Fluoride Film Subjected to Low Contact Stress," NASA TP 1584, 1980.
10. Bowden, F. P., and Tabor, D., The Friction and Lubrication of Solids, Clarendon Press, Oxford, England, 1950.
11. Burwell, J. T., and Strang, C. D., "On the Empirical Law of Adhesive Wear," Journal of Applied Physics, Vol. 23, No. 1, Jan. 1952, pp. 18-28.
12. Archard, J. F., "Contact and Rubbing of Flat Surfaces," Journal of Applied Physics, Vol. 24, No. 8, Aug. 1953, pp. 981-988.
13. Tonn, W., "Beitrag Zur Kenntnis des Verschleissvorganges Beim Kurzversuch," Zeitschrift fur Metallkunde, Vol. 29, June 1937, pp. 196-198.
14. Schallamach, A., and Turner, D. N., "The Wear of Slipping Wheels," Wear, Vol. 3, 1960, pp. 1-25.
15. Rabinowicz, E., Friction and Wear of Materials, Wiley, New York, 1965.
16. Kruschov, M. M., "Resistance of Metals to Wear by Abrasion, as Related to Hardness," Proceedings of the Conference on Lubrication and Wear, Institute of Mechanical Engineers, London, 1957, pp. 655-659.
17. Burwell, J. T., Jr., "Survey of Possible Wear Mechanisms," Wear, Vol. 1, Oct. 1957, pp. 119-141.
18. Yoshimoto, G., and Tsukizoe, T., "On the Mechanisms of Wear Between Metal Surfaces," Wear, Vol. 1, 1957-1958, pp. 471-490.
19. Kragelskii, I. V., Friction and Wear, Butterworths, London, 1965.
20. Bayer, R. G., Clinton, W. C., Nelson, C. W., and Schumacher, K. A., "Engineering Model for Wear," Wear, Vol. 5, 1962, pp. 378-391.
21. Suh, N. P., "The Delamination Theory of Wear," Wear, Vol. 25, 1973, pp. 111-124.
22. Vingsbo, O., "Wear and Wear Mechanisms," Wear of Materials, American Society of Mechanical Engineers, New York, 1979, pp. 620-635.
23. Fusaro, R. L., and Sliney, H. E., "Lubricating Characteristics of Polyimide and Polyimide-Bonded Graphite Fluoride Thin Films," American Society of Lubrication Engineers, Transactions, Vol. 16, No. 3, July 1973, pp. 189-196.
24. Fusaro, R. L., "Effect of Atmosphere and Temperature on Wear, Friction and Transfer of Polyimide Films," American Society of Lubrication Engineers, Transactions, Vol. 21, No. 2, Apr. 1978, pp. 125-132.

TABLE I. - SUMMARY OF EXPERIMENTAL DATA AND RESULTS

Load, N	Rider contact area, cm ²	Projected rider contact stress		Average value of friction coefficient at:				Test duration, kc	Thickness of film worn through, μm	Film wear rate, m ³ /m
		MPa	psi	5 kc	60 kc	500 kc	End test			
2.5	0.0035	7	1000	0.12	0.15	0.15	0.16	1 190	13	0.8x10 ⁻¹⁴
4.9	0.0035	14	2000	0.12	0.14	0.18	0.19	565	15	2.3x10 ⁻¹⁴
	.0071	7	1000	.14	.17	.19	.22	6 915	15	.29x10 ⁻¹⁴
	.0145	3.5	500	.16	.19	.15	.34	7 930	13	.25x10 ⁻¹⁴
	.0240	2.0	300	.15	.19	.19	.20	10 300	8	.14x10 ⁻¹⁴
9.8	0.0035	28	4000	0.14	0.16	---	0.16	400	15	2.9x10 ⁻¹⁴
	.0071	14	2000	.13	.19	.22	.28	3 500	39	1.7x10 ⁻¹⁴
	.0145	7	1000	.16	.20	.23	.23	11 670	30	.60x10 ⁻¹⁴
	.0240	4.1	600	.16	.21	.34	.29	4 340	10	.27x10 ⁻¹⁴
14.7	0.0035	42	6000	0.13	0.22	0.22	0.22	500		5.5x10 ⁻¹⁴
	.0071	21	3000	.13	.19	.16	.20	690	14	2.6x10 ⁻¹⁴
19.6	0.0035	56	8000	0.13	0.13	---	0.13	65	23	46.0x10 ⁻¹⁴
	.0071	28	4000	.14	.15	.17	.18	800	21	4.9x10 ⁻¹⁴
	.0145	14	2000	.16	.24	.28	.26	1 110	16	2.4x10 ⁻¹⁴
	.0240	8.1	1200	.16	.20	.19	.31	2 200	25	2.2x10 ⁻¹⁴
29.4	0.0071	42	6000	0.13	0.13	---	0.13	45	21	55.0x10 ⁻¹⁴
	.0145	21	3000	.16	.26	---	.22	112	10	12.0x10 ⁻¹⁴
	.0240	12	1800	.17	.24	.28	.25	910	27	6.1x10 ⁻¹⁴
34.4	0.0145	28	4000	0.14	0.18	---	0.16	90	14	34.0x10 ⁻¹⁴
39.2	0.0240	16	2300	0.16	0.19	---	0.18	220	25	24.0x10 ⁻¹⁴
58.8	0.0240	24	3500	0.16	---	---	0.18	20	14	121.0x10 ⁻¹⁴

TABLE II. - TEMPERATURE RISE ON FILM WEAR TRACK DUE TO FRICTIONAL HEATING

Load,	Rider contact area, cm ²	Projected rider contact stress		Film temperature (°C) at sliding durations of:							
		MPa	psi	20	60	200	500	1000	2000	4000	End test
2.5	0.0035	7	1000	25°	28°	30°	31°	31°	---	---	31°
4.9	0.0035	14	2000	30°	34°	34°	34°	---	---	---	35°
	.0071	7	1000	28°	32°	33°	35°	35°	36°	34°	34°
	.0145	3.5	500	31°	34°	34°	34°	34°	34°	40°	40°
	.0240	2.0	300	29°	32°	34°	33°	33°	37°	36°	37°
9.8	0.0035	28	4000	31°	35°	35°	---	---	---	---	36°
	.0071	14	2000	30°	34°	42°	44°	43°	42°	43°	43°
	.0145	7	1000	33°	38°	42°	48°	50°	49°	50°	50°
	.0240	4.1	600	---	---	---	40°	---	48°	---	48°
14.7	0.0035	42	6000	---	---	---	---	---	---	---	---
	.0071	21	3000	38°	48°	57°	57°	---	---	---	54°
19.6	0.0035	56	8000	42°	48°	---	---	---	---	---	48°
	.0071	28	4000	41°	51°	58°	59°	---	---	---	57°
	.0145	14	2000	45°	60°	63°	65°	64°	---	---	64°
	.0240	8.1	1200	38°	60°	58°	61°	60°	56°	---	56°
29.4	0.0071	42	6000	45°	---	---	---	---	---	---	54°
	.0145	21	3000	---	---	---	---	---	---	---	71°
	.0240	12	1800	---	72°	80°	77°	---	---	---	69°
34.9	0.0145	28	4000	42°	74°	---	---	---	---	---	67°
39.2	0.0240	16	2300	56°	86°	---	---	---	---	---	87°
58.8	0.0240	24	3500	49°	---	---	---	---	---	---	49°

TABLE III. - COMPARISON OF POLYIMIDE-BONDED GRAPHITE FLUORIDE
FILM WEAR RATES AS A FUNCTION OF LOAD AND RIDER CONTACT AREA

Total load		Rider contact area, cm ²			
N	lb	0.0035	0.0071	0.0145	0.0240
		Film wear rate, m ³ /m			
2.5	0.55	0.8x10 ⁻¹⁴	-----	-----	-----
4.9	1.1	2.3x10 ⁻¹⁴	0.29x10 ⁻¹⁴	0.25x10 ⁻¹⁴	0.14x10 ⁻¹⁴
9.8	2.2	2.9x10 ⁻¹⁴	1.7x10 ⁻¹⁴	.60x10 ⁻¹⁴	.27x10 ⁻¹⁴
14.7	3.3	5.5x10 ⁻¹⁴	2.6x10 ⁻¹⁴	-----	-----
19.6	4.4	4.6x10 ⁻¹⁴	4.9x10 ⁻¹⁴	2.4x10 ⁻¹⁴	2.2x10 ⁻¹⁴
29.4	6.6	-----	5.5x10 ⁻¹⁴	12x10 ⁻¹⁴	6.1x10 ⁻¹⁴
34.3	7.7	-----	-----	34x10 ⁻¹⁴	-----
39.2	8.8	-----	-----	-----	24x10 ⁻¹⁴
58.8	13.2	-----	-----	-----	124x10 ⁻¹⁴

TABLE IV. - COMPARISON OF POLYIMIDE-BONDED GRAPHITE FLUORIDE FILM
WEAR RATES AS A FUNCTION OF CONTACT STRESS AND RIDER CONTACT AREA

Contact stress (pressure)		Rider contact area, cm ²			
MPa	psi	0.0035	0.0071	0.0145	0.0240
		Film wear rate, m ³ /m			
2.0	300	-----	-----	-----	0.14x10 ⁻¹⁴
3.5	500	-----	-----	0.25x10 ⁻¹⁴	-----
4.1	600	-----	-----	-----	0.27x10 ⁻¹⁴
7.0	1000	0.80x10 ⁻¹⁴	0.29x10 ⁻¹⁴	0.60x10 ⁻¹⁴	-----
8.1	1200	-----	-----	-----	2.2x10 ⁻¹⁴
12	1800	-----	-----	-----	6.1x10 ⁻¹⁴
14	2000	2.3x10 ⁻¹⁴	1.7x10 ⁻¹⁴	2.4x10 ⁻¹⁴	-----
16	3000	-----	-----	-----	24x10 ⁻¹⁴
21	3000	-----	2.6x10 ⁻¹⁴	12x10 ⁻¹⁴	-----
24	3500	-----	-----	-----	124x10 ⁻¹⁴
28	4000	2.9x10 ⁻¹⁴	4.9x10 ⁻¹⁴	34x10 ⁻¹⁴	-----
42	6000	5.5x10 ⁻¹⁴	5.5x10 ⁻¹⁴	-----	-----
56	8000	4.6x10 ⁻¹⁴	-----	-----	-----

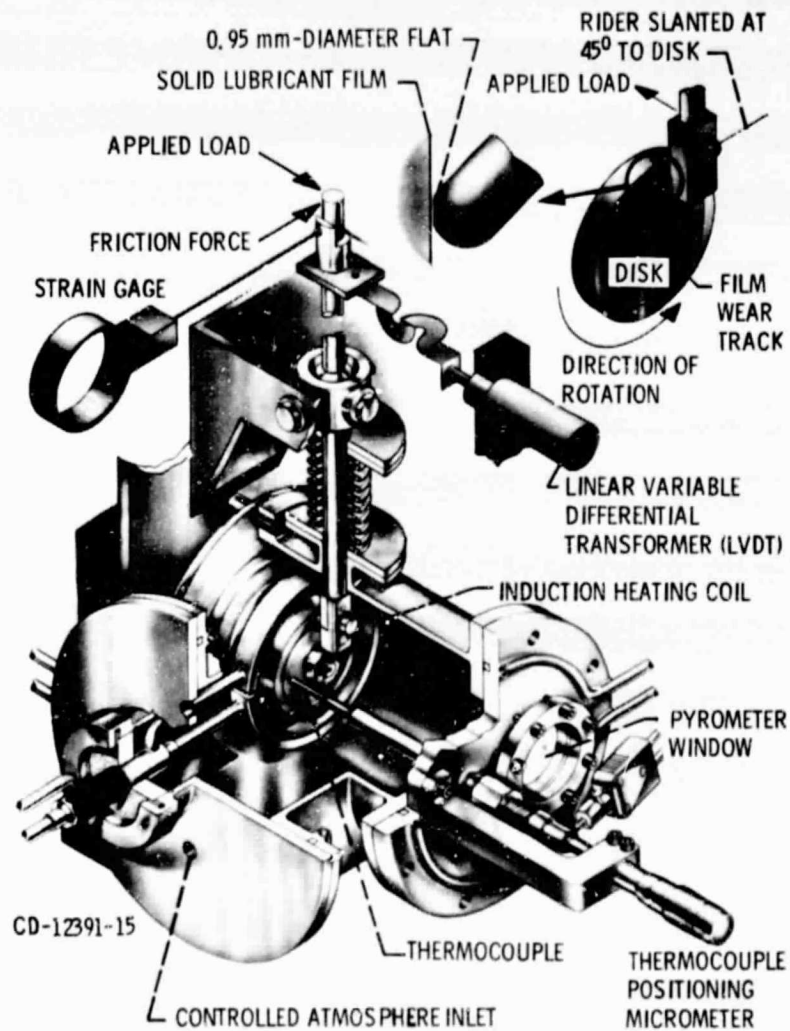


Figure 1. - Friction and wear apparatus.

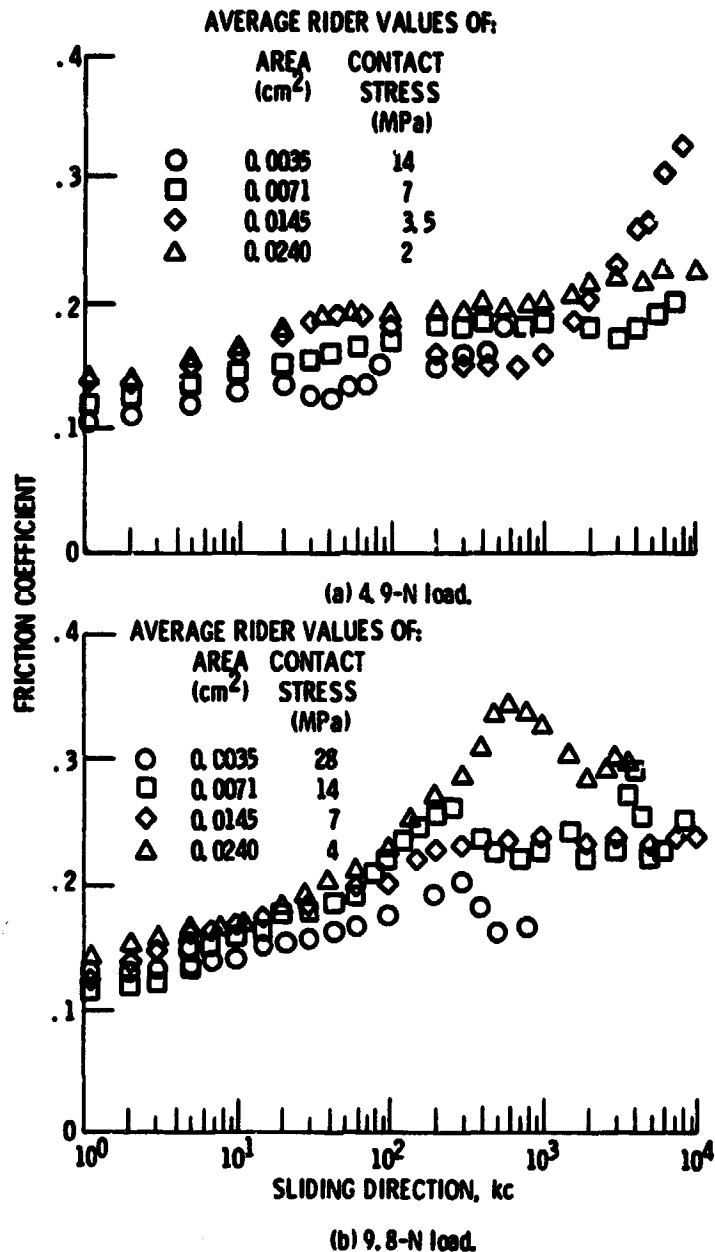


Figure 2. - Effect of rider contact area and projected contact stress on the friction coefficient of polyimide-bonded graphite fluoride films as a function of sliding duration for loads of (a) 4.9-N, (b) 9.8-N, (c) 19.6-N, and (d) 29.4-N.

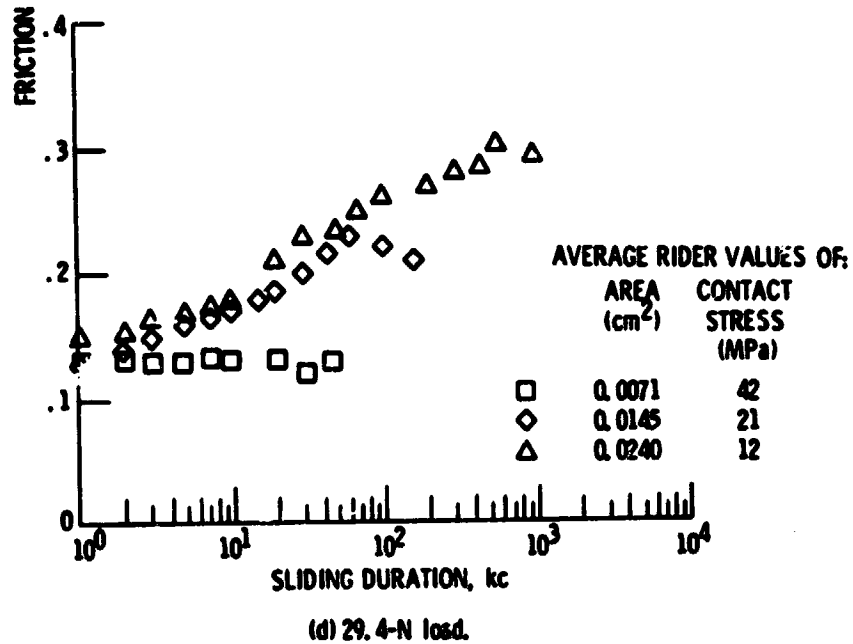
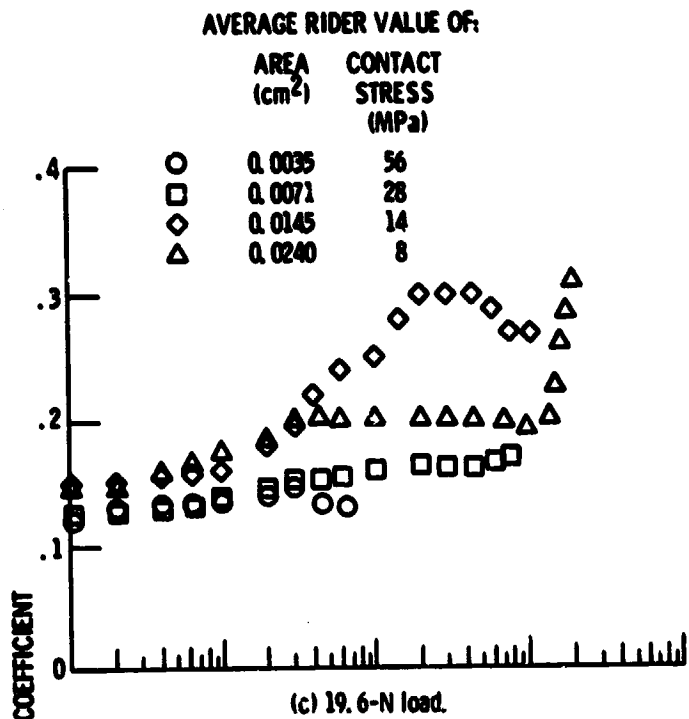


Figure 2. - Concluded.

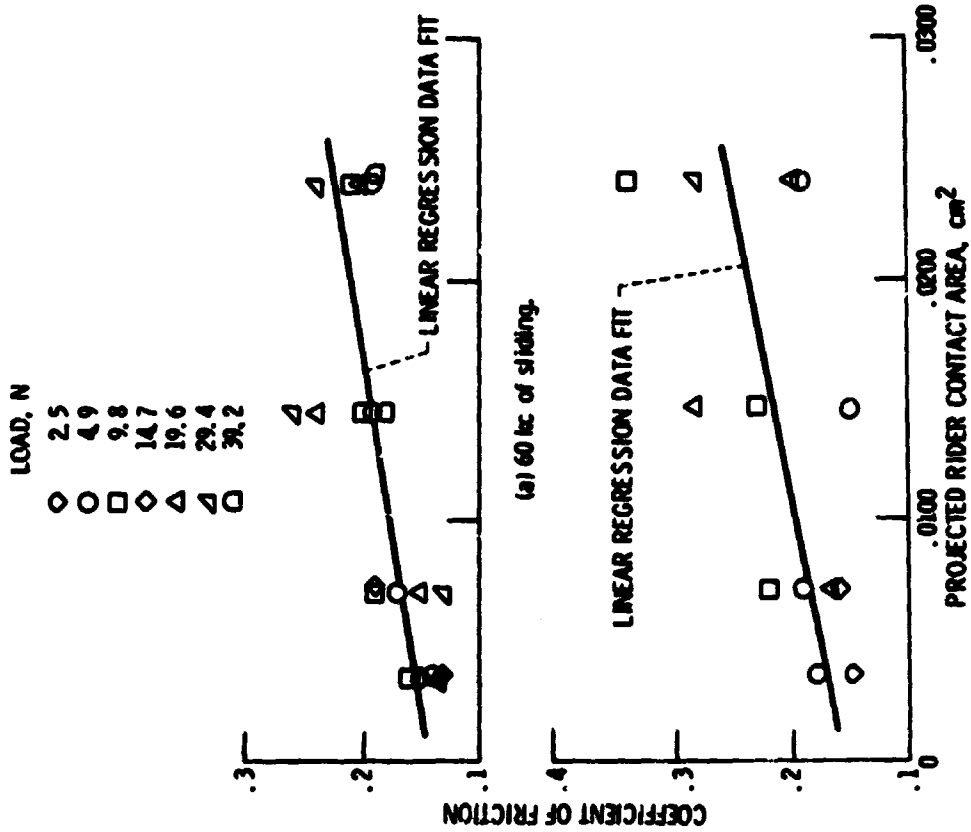


Figure 3. - Friction coefficient as a function of projected rider contact area for 440 C stainless steel riders sliding on PI-bonded graphite fluoride films under various loads.

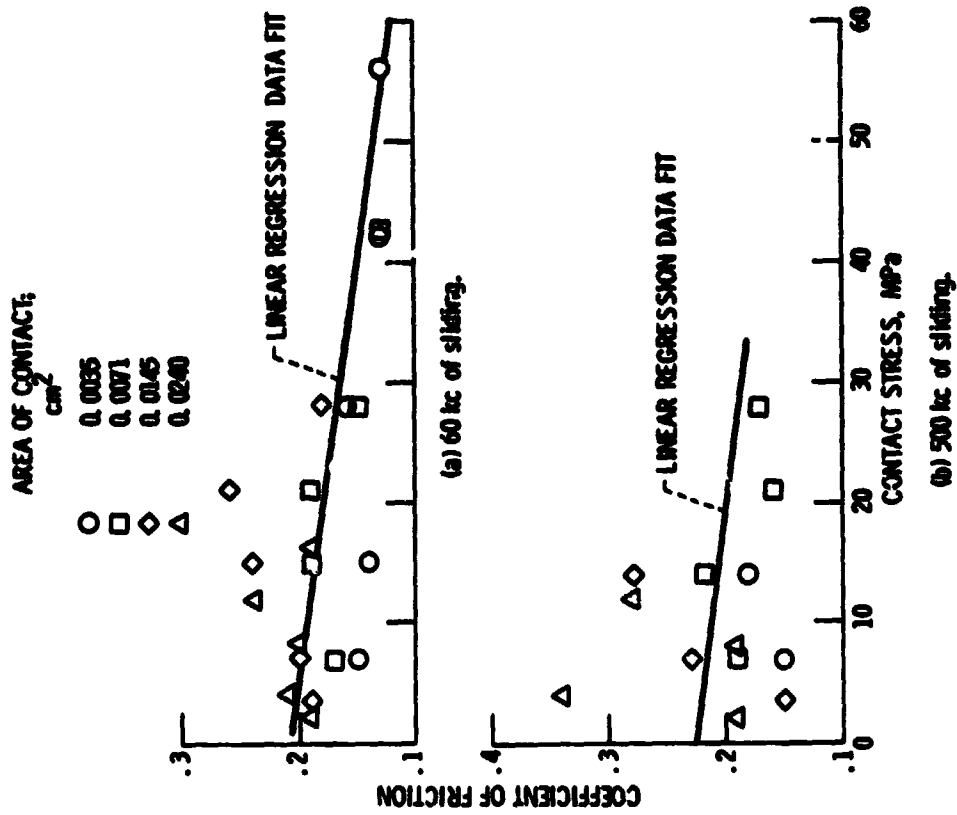


Figure 4. - Friction coefficient as a function of contact stress (pre-sure) for 440 C stainless steel riders with different contact areas sliding against PI-bonded graphite fluoride films.

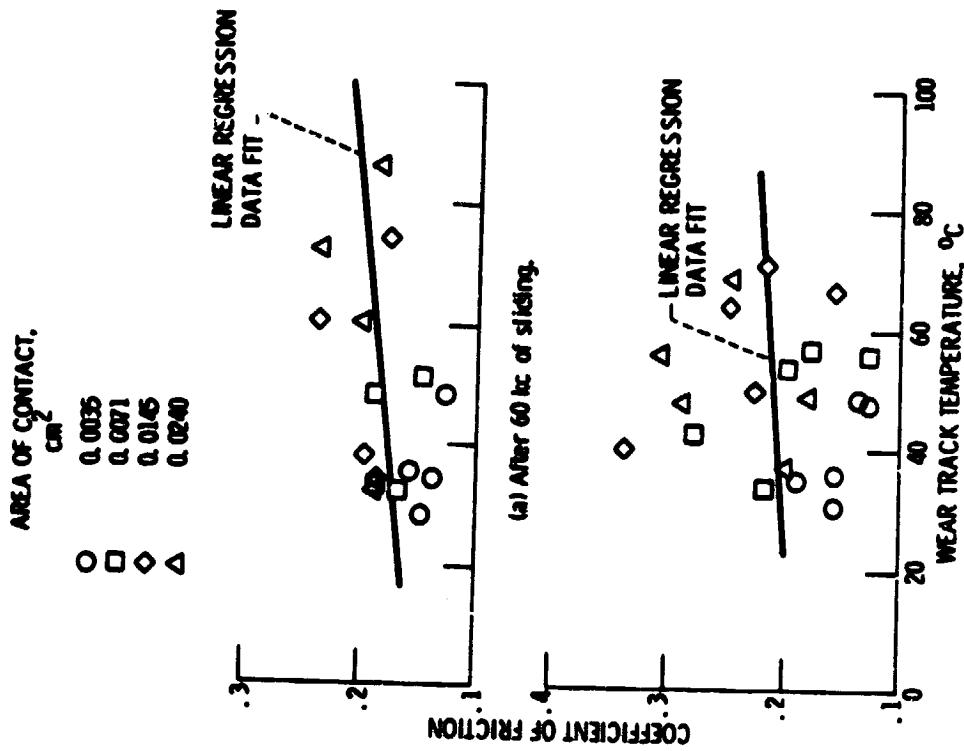


Figure 5. - Friction coefficient as a function of film wear track temperature for 400 C stainless steel riders with different contact areas sliding on PI-bonded graphite fluoride films under various loads.

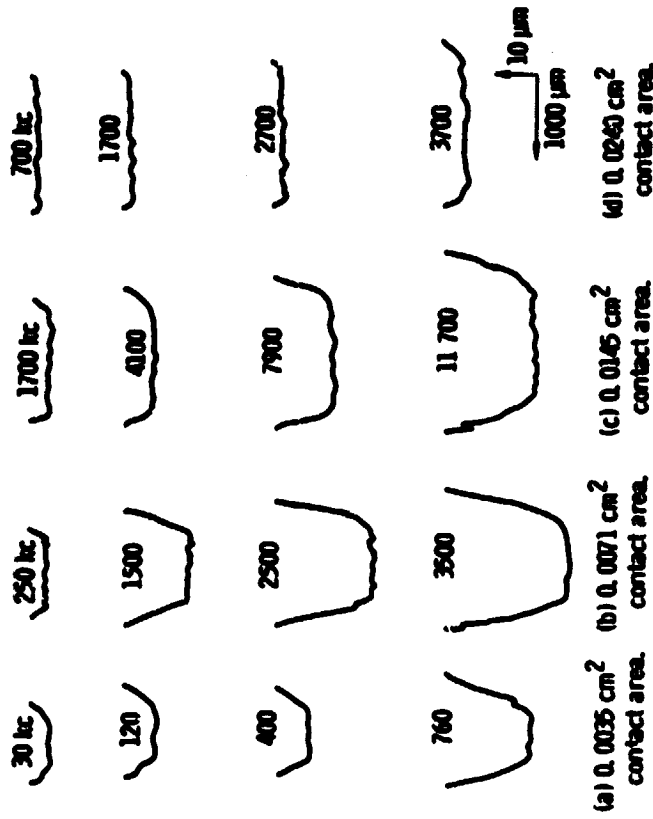


Figure 6. - Surface profiles of the wear tracks on polyimide-bonded graphite fluoride films after various sliding durations. The wear tracks were produced by sliding riders with different areas of contact against the films under a 9.8-N load at 1000 rpm.

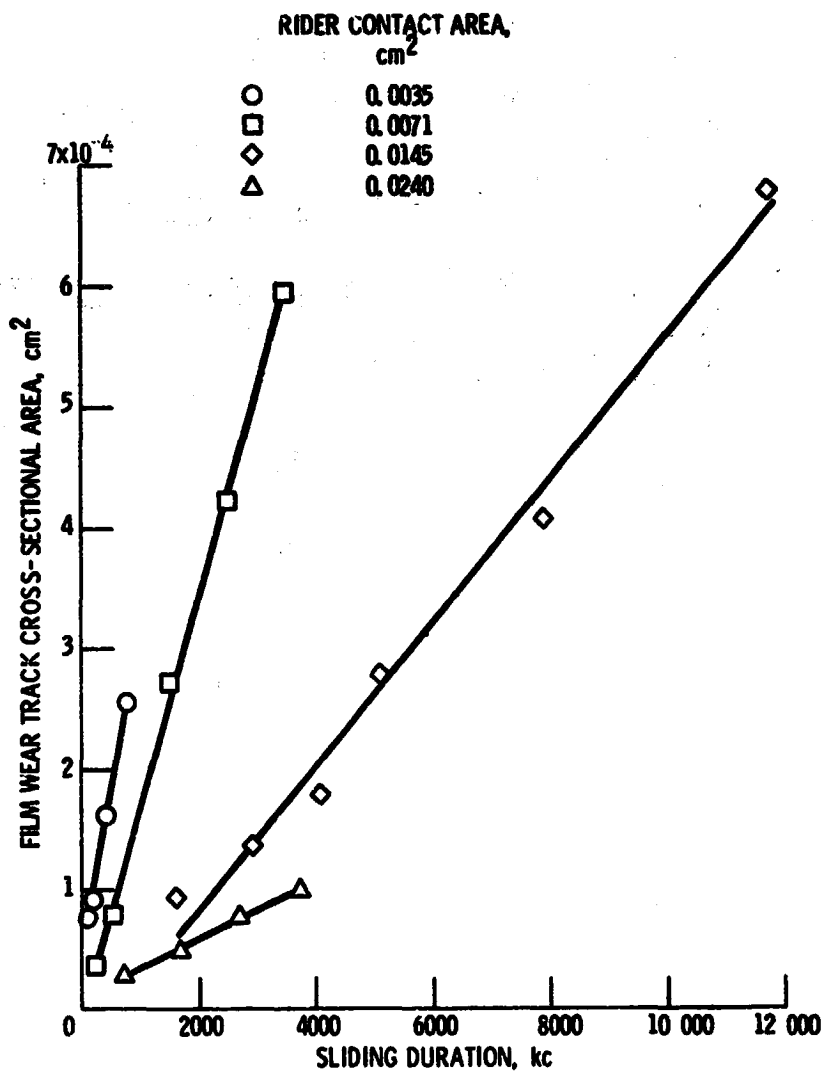


Figure 7. - Polyimide-bonded graphite fluoride film wear as a function of sliding duration for a 9.8-N load applied to four different rider contact areas.

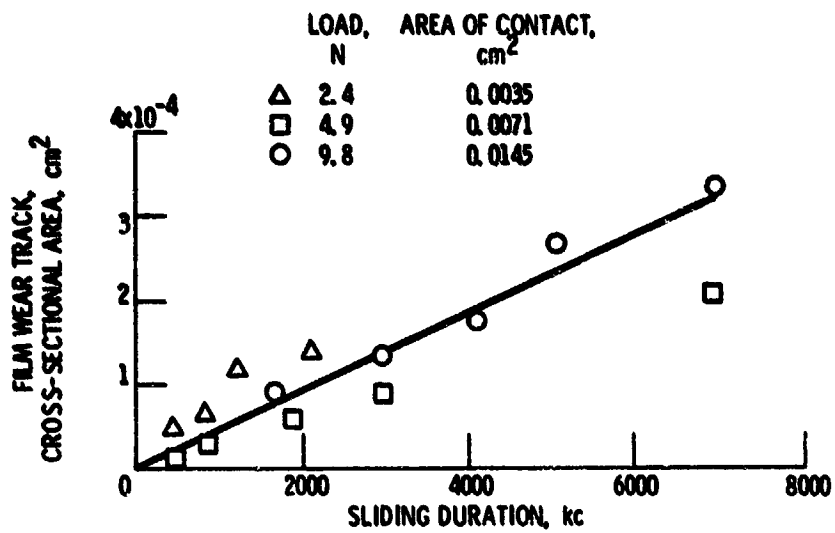


Figure 8 - Polyimide-bonded graphite fluoride film wear as a function of sliding duration for a constant contact stress of 7.0 MPa (1000 psi) which was obtained by using various loads and areas of contact.

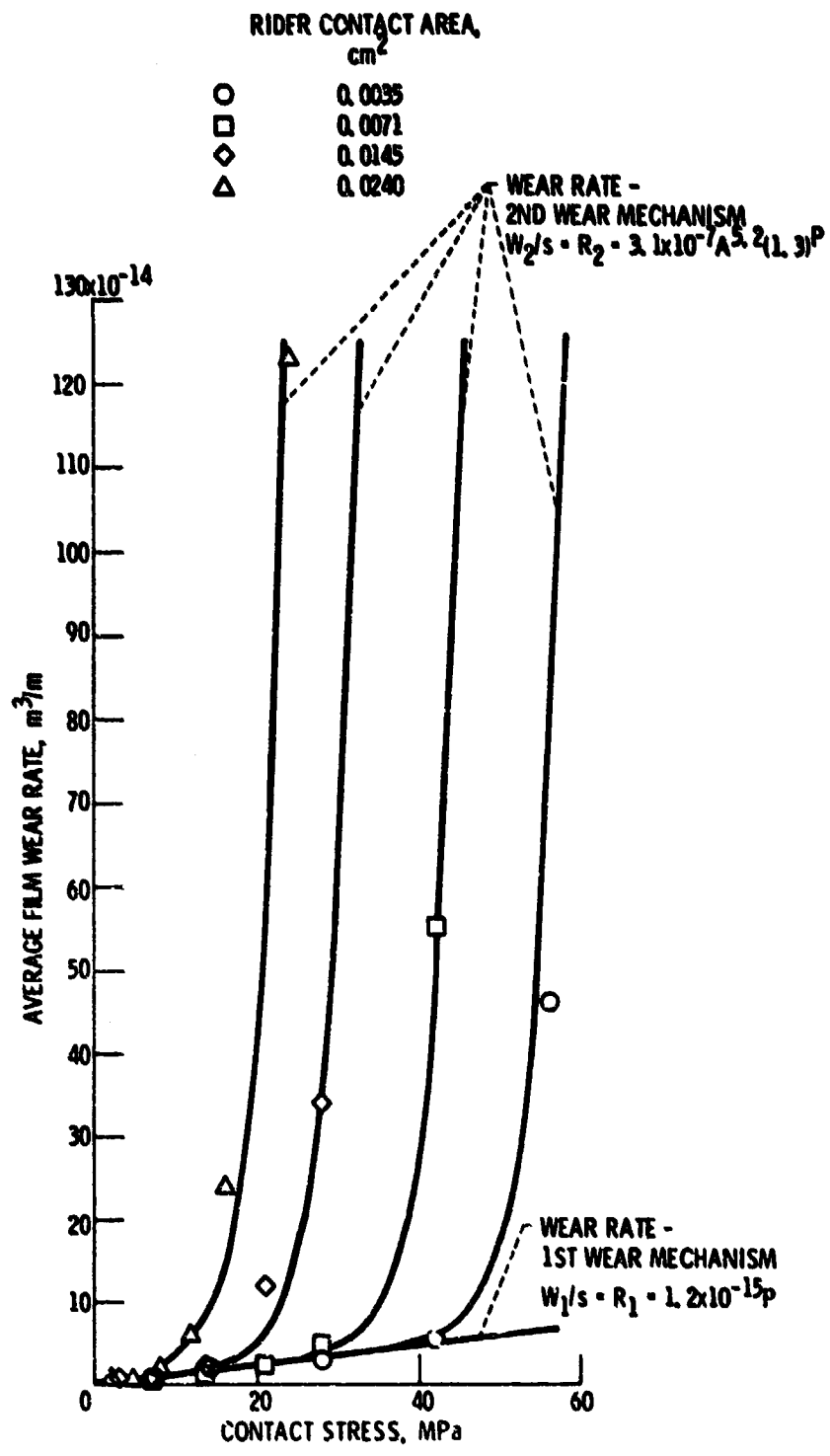


Figure 9. - Average PI-bonded (CF_x) film wear rate experimental values as a function of contact stress showing wear rate curves which were derived from the data points.

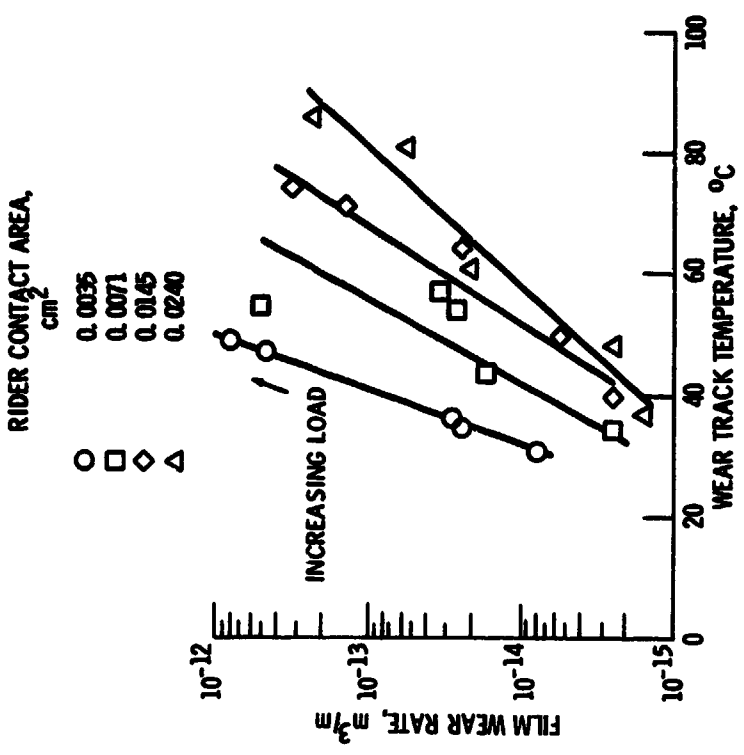


Figure 10. - Average film wear attributed to the second wear mechanism as a function of contact stress showing wear rate curves which were fitted to the data by exponential least square techniques.

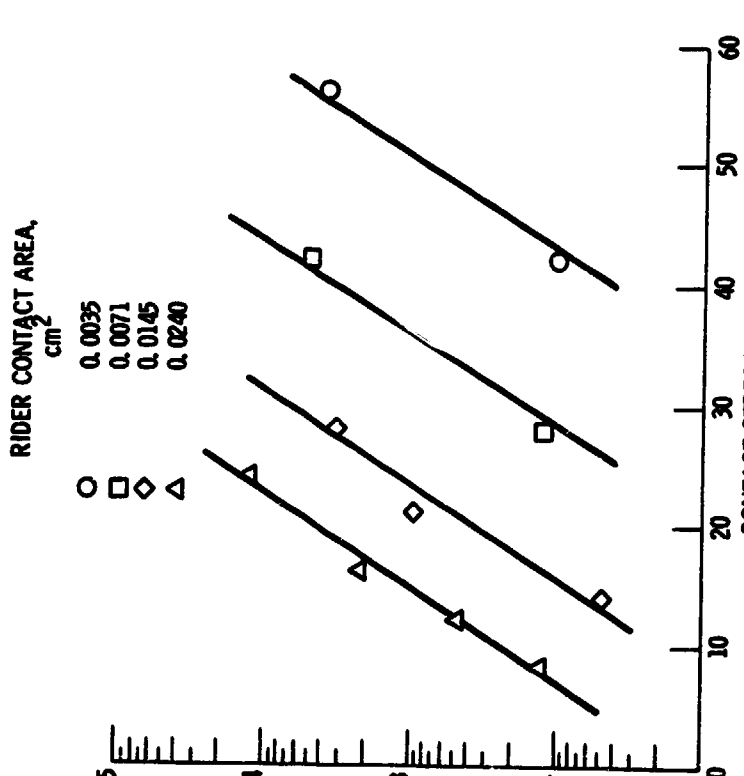
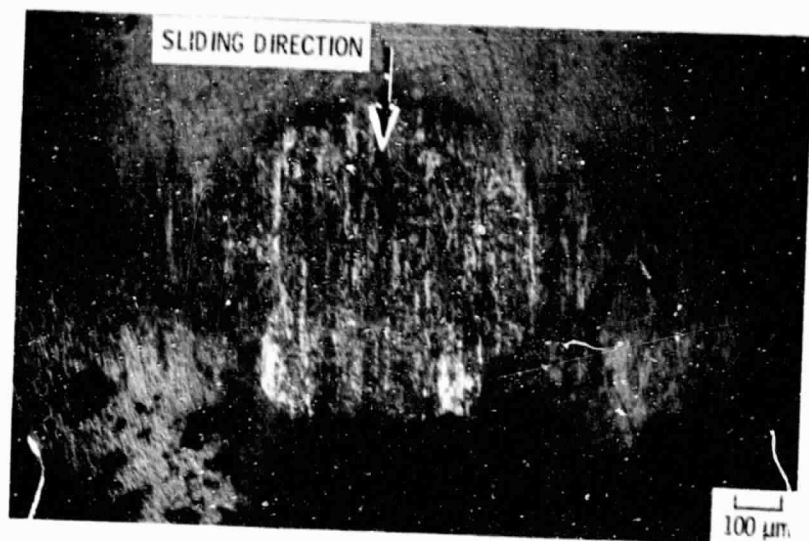
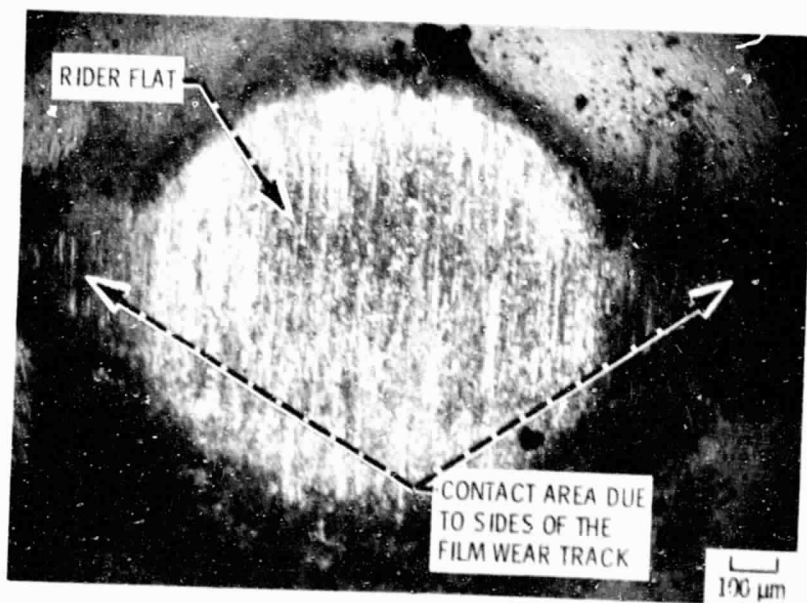


Figure 11. - Film wear rate as a function of maximum wear track temperature for 440 C HT stainless steel riders sliding on P1-bonded (CF_x)_n films under various loads and rider contact areas.



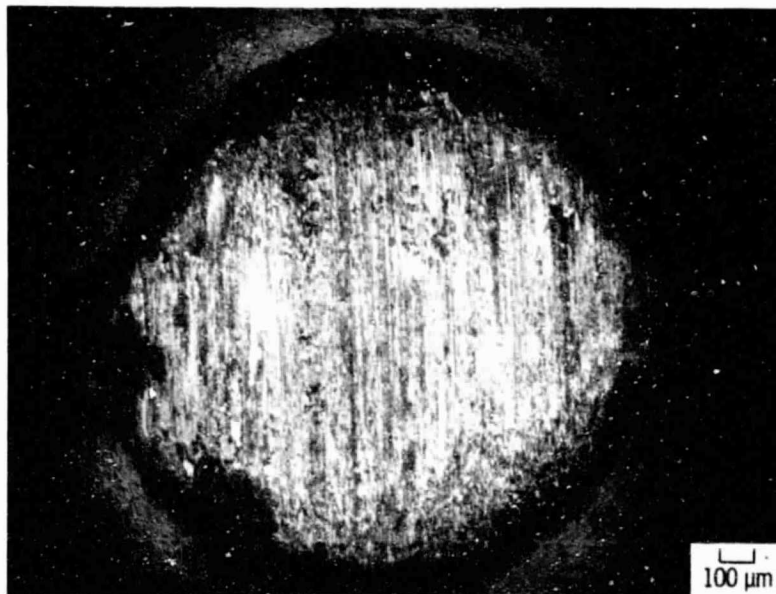
(a) 0.0035 cm²-AREA FLAT. (760 kc OF SLIDING.)



(b) 0.0071 cm²-AREA FLAT. (3500 kc OF SLIDING.)

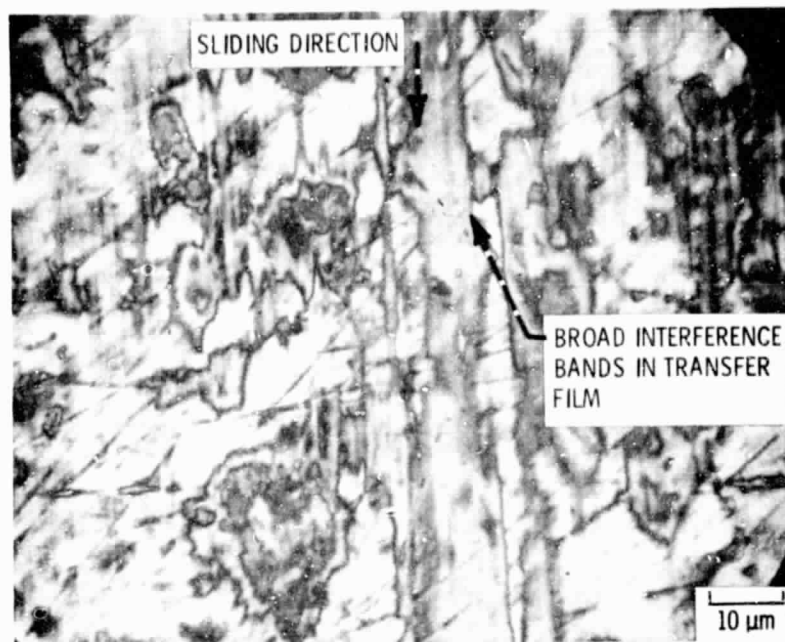
Figure 12. - Photomicrographs of rider contact areas after various intervals of sliding under a 9.8-N load showing the contact made by the sides of the wear track.

ORIGINAL PAGE
OF MICROFILM



(c) 0.0145 cm²-AREA FLAT. (4100 kc OF SLIDING.)

Figure 12. - Concluded.



(a) 1 kc OF SLIDING, $\mu = 0.12$.



(b) 6900 kc OF SLIDING, $\mu = 0.20$.

Figure 13. - Photomicrographs of the transfer to the 0.0071 cm^2 -area rider flat after (a) 1 kc of sliding and (b) 6900 kc of sliding for the 4.9-N load applied to the flat.

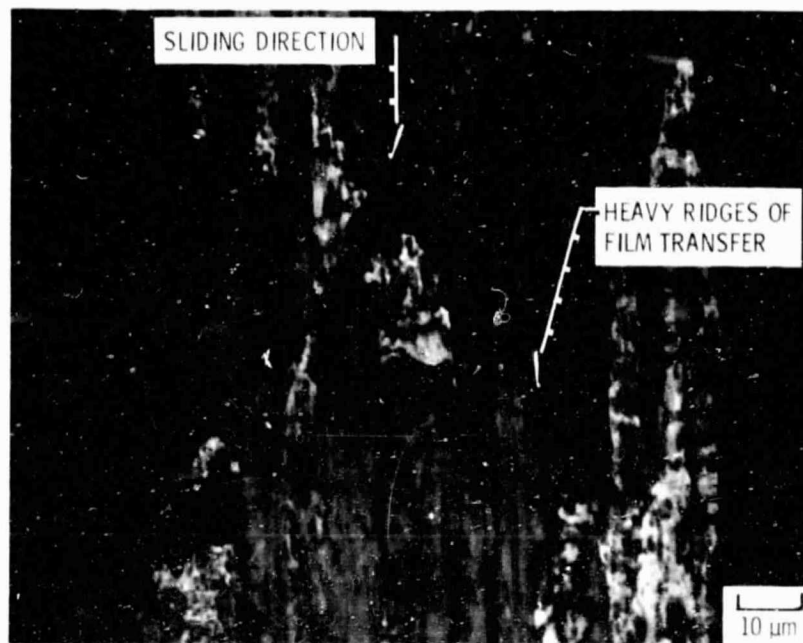
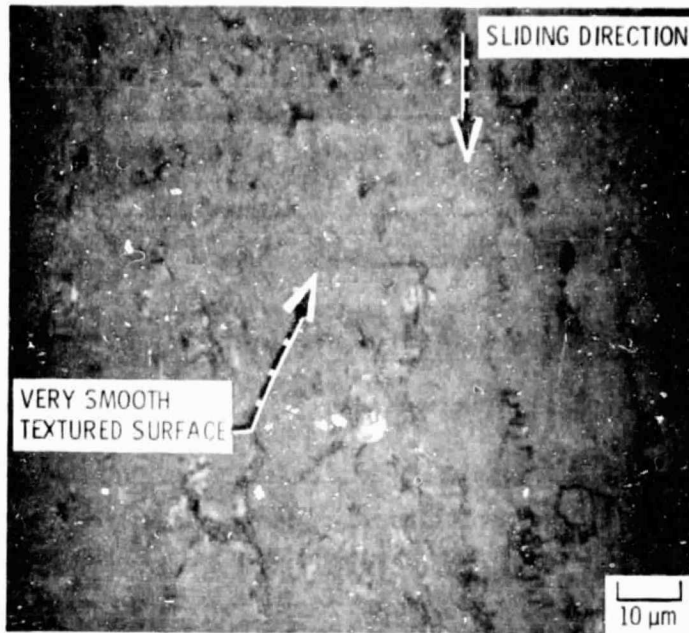
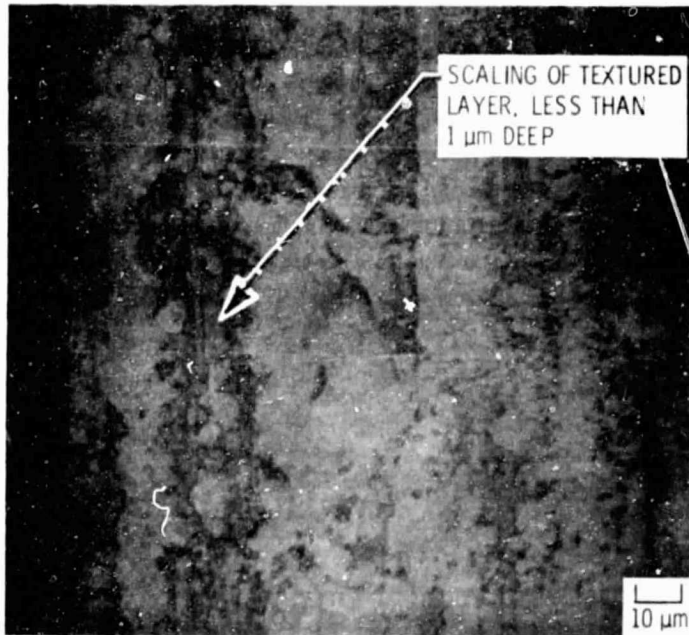


Figure 14. - Photomicrograph of the transfer to the 0.0145-cm^2 -area rider flat after 7900 kc of sliding for the 4.9-N load applied to the flat. ($\mu = 0.33$.)



(a) 4.9-N LOAD, 3000 kc OF SLIDING.



(b) 9.8-N LOAD, 3500 kc OF SLIDING.

Figure 15. - Photomicrographs of the film wear tracks showing the effect of load (at a constant area of contact of 0.0071-cm^2) on film wear.